Batteries & Supercaps

Research Article
doi.org/10.1002/batt.202200458

Chemistry Europe
European Chemical Societies Publishing

www.batteries-supercaps.org

Special Collection

Low-Temperature and High-Areal-Capacity Rechargeable Lithium Batteries enabled by π-Conjugated Systems

Liwei Cheng,[a] Xinyu Sun,[a] Gongkai Wang,*[b] Yuhua Chen,[c] Qiaonan Zhu,[a] Pengfei Hu,[a] Wei Zhou,[a] and Hua Wang*[a]

High mass loading and high areal capacity are essential for lithium-ion batteries (LIBs) with high energy density, but they usually suffer from the sluggish charge-transfer kinetic of thick electrodes, especially at low temperature. Here, organic molecule perylene-3,4,9,10-tetracarboxylic dianhydride (PTCDA) has been investigated as a feasible cathode for high areal capacity rechargeable LIBs operated at low temperature. Specifically, the charge storage process mainly occurs on the surface redox-active groups of PTCDA, resulting in a fast kinetics of charge storage. Meanwhile, the delocalization of electrons in the π-conjugated systems of PTCDA could enhance the electron transportation prominently. Consequently, the Li-PTCDA battery with a high mass loading of 14.35 mg cm^{-2} delivers a high reversible areal capacity of 1.06 mAh cm^{-2} at −40 °C. This work demonstrates a great potential of π-conjugated organic materials for low temperature and high-areal-capacity rechargeable LIBs.

Introduction

High areal capacity is a key metric for commercial LIBs, which requires thick electrodes with high mass loading of active materials.[1–4] However, owing to the significant decrease in the ionic and electronic conduction of the thick electrode, high mass loading electrodes usually undergo sluggish kinetics and low utilization of active materials, which will be deteriorated when the operating temperature drops below 0 °C .[5–8] At low temperature, the ionic diffusion is largely restrained due to an insufficient dynamics, leading to a rapid decrease in capacity, rate capability and cyclic stability.[9–11] Recently, many works have been devoted to enhance the ionic diffusion rate within the bulk electrode at low temperature through electrode-structure design, but it inevitably sacrifices the mass loading of active materials and thus a decreased energy density.[12–14] Hence, it is a challenge to develop high-areal-capacity rechargeable LIBs at low temperature.

To improve the kinetics and utilization of active materials on high mass loading electrode at low temperature, it is essential to investigate appropriate electrode with high ionic and electronic conduction. Conventional inorganic cathode undergoes lattice contraction as the temperature drops, which limits the diffusion of Li-ions in the crystal and leads to sluggish ion transport kinetics.[15–17] Compared to rigid inorganic materials, the charge storage of organic compounds mainly locates on the surface moieties or in the large interstitial space of the flexible solids, facilitating the fast charge storage kinetics.[18–21] Moreover, many redox active organic materials have π-conjugated system due to the large aromatic carbon.[22–25] The delocalization of electrons in the π-conjugated structure endows the molecule with an electron-rich feature, which prominently enhance the electronic conductivity of organics.[26–30] Hence, π-conjugated organic materials could be highly suitable for low temperature and high-areal-capacity LIBs, therefore, exploration of adequate organic cathodes is urgently needed.

Herein, we present a high-areal-capacity rechargeable low temperature LIBs based on the PTCDA cathode. PTCDA is a kind of aromatic anhydride containing C=O redox-active centers, with a high theoretical specific capacity of 131 mAh g^{-1} for Li-ions storage.[31,32] The charge storage of surface C=O redox active groups is beneficial for the rapid Li-ions storage, and the electrons delocalization of the π-conjugated system enables PTCDA a highly conductive cathode material, synergistically giving rise to the excellent low temperature electrochemical performance of PTCDA with a high mass loading. As a result, the PTCDA cathode with a high mass loading of 14.35 mg cm^{-2} exhibits a superior areal capacity of 1.06 mAh cm^{-2} at −40 °C. This work demonstrates that π-conjugated organic materials are potential cathodes for high-areal-capacity rechargeable LIBs at low temperature.

[a] L. Cheng, X. Sun, Q. Zhu, Dr. P. Hu, Prof. W. Zhou, Prof. H. Wang
School of Chemistry
Beihang University
Beijing 100191, China
E-mail: wanghua8651@buaa.edu.cn
[b] Prof. G. Wang
School of Material Science and Engineering, Tianjin Key Laboratory of Materials Laminating Fabrication and Interface Control Technology
Hebei University of Technology
Tianjin 300130, China
E-mail: wang.gongkai@hebut.edu.cn
[c] Y. Chen
State Key Laboratory of Space Power-sources Technology
Shanghai Institute of Space Power-Sources
Shanghai, 200245, China

Supporting information for this article is available on the WWW under https://doi.org/10.1002/batt.202200458

Special Collection An invited contribution to a Special Collection on Organic Batteries

Research Article
doi.org/10.1002/batt.202200458
Chemistry Europe
European Chemical Societies Publishing

Results and Discussion

According to the electrostatic potential (ESP) mapping of PTCDA molecule, the blue regions around O atoms are rich in electron density, which are considered as reactive reaction sites (Figure 1a). The C=O bonds in the PTCDA are favorable for Li-ions uptake and could transform to C–O–Li when the storage process occurs (Figure S1). The current density susceptibility of PTCDA is visualized that the π-ring current encircles the ring system around the ring plane (Figure 1b). The delocalization of electrons in the π-conjugated system makes PTCDA an electron-rich feature over a large area, thus leading to a good electronic conductivity. The highly conductive and the well-defined redox-active moieties of π-conjugated PTCDA may be the prerequisites for its high performance at low temperature (Figure 1c).

In order to enhance the electrochemical performance of Li-PTCDA battery, the commercially available red PTCDA (R-PTCDA) powder was annealed at 450 °C to further increase its electronic conductivity while minimizing the decomposition of PTCDA (Figures S2 and S3).[33,34] After annealing process, the XRD pattern shows the formation of α-phase PTCDA (B-PTCDA) (Figure 2a).[4] As shown in the (102) plane of B-PTCDA, the redox active C=O groups are located at the surface, and a large interstitial space is also observed between two adjacent molecules, which facilitate the rapid Li-ions storage (Figure 2b).[35] Although the color of PTCDA changed from red to brown after the annealing process, the Fourier transform infrared spectroscopy (FTIR) shows that there is no significant difference between the red and brown ones, indicating that the PTCDA does not decompose or generates perylene tetraradicals at this process.[34] The evolutions of PTCDA molecule were also monitored by X-ray photoelectron spectroscopy (XPS). For the C1s XPS (Figure 2c), the peak assigned to C=O bond (288.6 eV) of B-PTCDA is weakened, indicating the polymerization of PTCDA. Meanwhile, the similar phenomenon is also confirmed by the O1s region (Figure 2d). The intensity of C=O peak at 531.6 eV is reduced while the peak of C–O is strengthened after the annealing process. The polymerizations can effectively suppress the dissolution of small molecule PTCDA and extend the π-conjugated system, which is beneficial for the cycle stability and rate capability of the PTCDA-based battery.[4] Moreover, the scanning electron microscope (SEM) image implies that the B-PTCDA is in the shape of small piece with sizes of about 200–400 nm. Compared to the R-PTCDA, the reduced size is beneficial to increase the fast transport of Li-ion, enhancing the charge/discharge capability (Figure S4).

Then, the room temperature electrochemical performance of B-PTCDA cathode was investigated in advance. Regarding to its rate performance (Figure 3a), a high specific capacity of 130.4 mAh g^{-1} is achieved at 0.2 C (1 C = 131 mA g^{-1}), which almost reaches the theoretical capacity of PTCDA. As the current densities increase to 1 C and 10 C, the B-PTCDA still retains high reversible capacities of 122.8 and 77.6 mAh g^{-1},

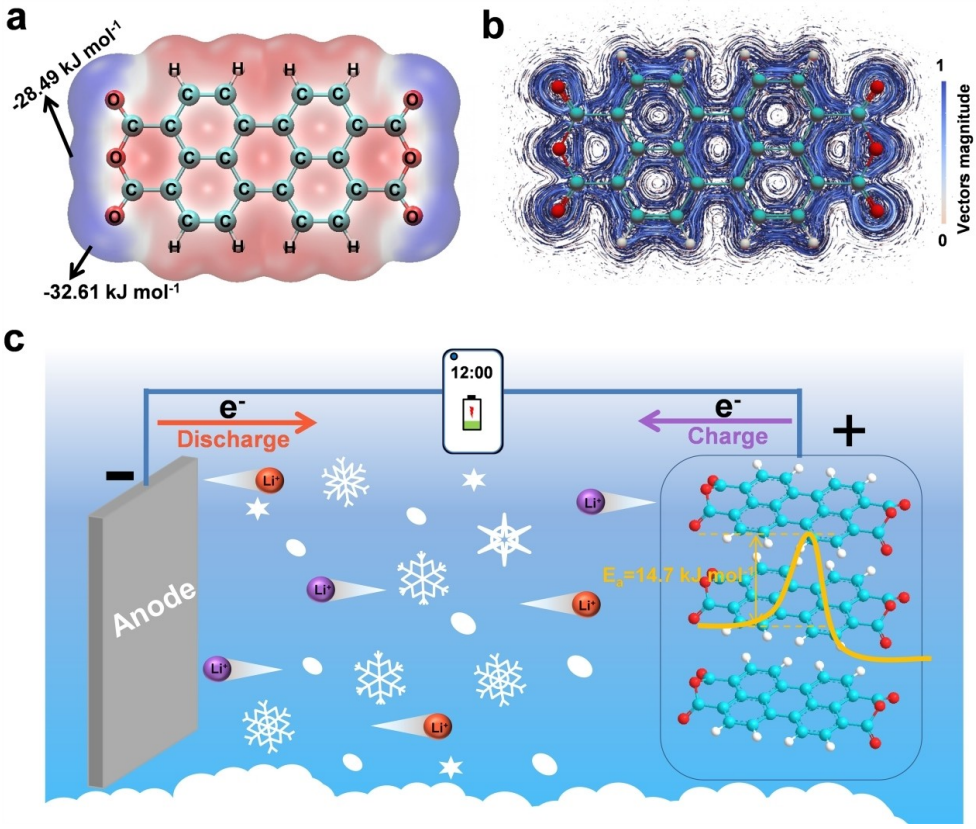

Figure 1. a) ESP mapping of PTCDA molecules. b) Magnetically induced current of PTCDA molecule by streamline representation. c) Schematic illustration of the PTCDA-based battery at low temperature.

Research Article
doi.org/10.1002/batt.202200458
Chemistry Europe
European Chemical Societies Publishing

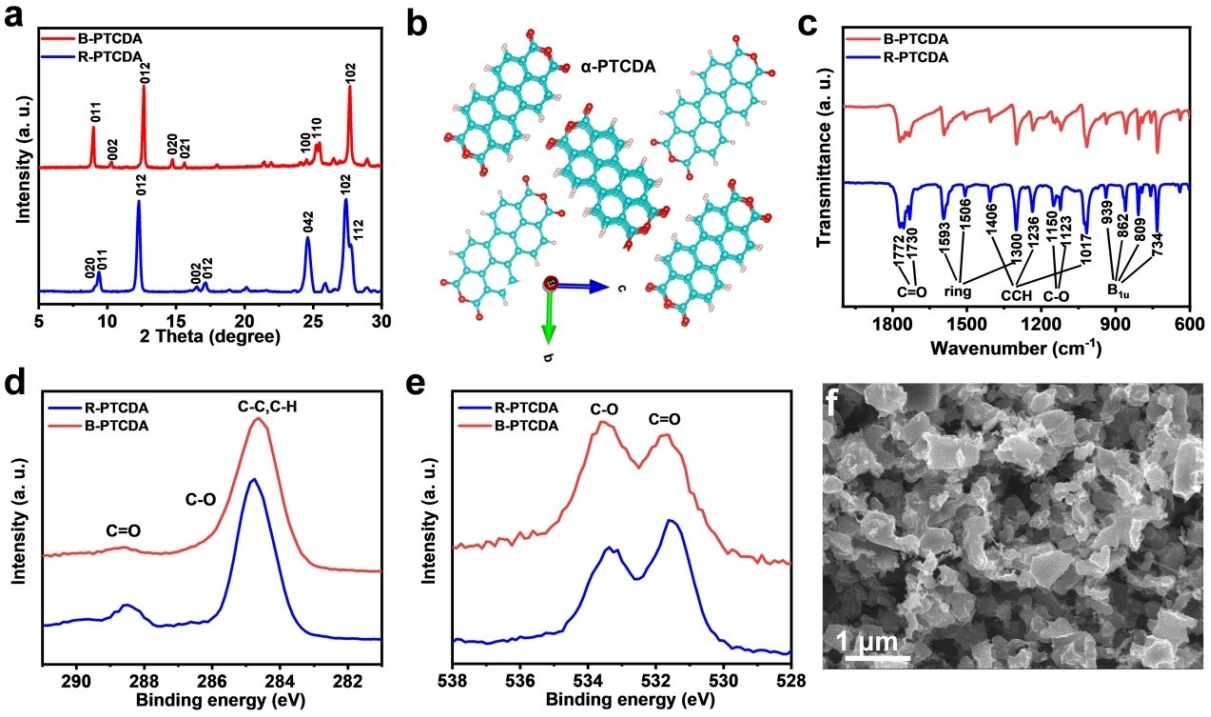

Figure 2. a) XRD patterns of PTCDA. b) Structure of the α-phase PTCDA. c) FTIR spectra of PTCDA. XPS analysis of d) C 1s and e) O 1s regions for PTCDA. f) SEM image of B-PTCDA.

which are about 94.2% and 59.5% of the capacity at 0.2 C. The specific capacity is restored to 126.9 mAh g^{-1} when the rate is switched back to 0.2 C. Moreover, obvious voltage platforms can be observed from the corresponding charge/discharge curves at different cycle rates, suggesting the superior rate capability of B-PTCDA cathodes (Figure 3b). According to the Ragone plot, the B-PTCDA electrode shows a high energy density of 316.7 Wh kg^{-1} at the power density of 159.8 W kg^{-1}, and an acceptable energy density of 169.8 Wh kg^{-1} at a superior power density of 2882 W kg^{-1}, which is comparable to commercialized LIBs (Figures 3c and S6). With respect to the galvanostatic charge/discharge (GCD) test at the current density of 1 C, the B-PTCDA cathode (Figure 3d) exhibits a high reversible capacity of 111.6 mAh g^{-1} after 100 cycles with a high capacity retention of 97.2%. Furthermore, after 1000 cycles at a higher rate of 8 C, a high capacity of 70.4 mAh g^{-1} can be still achieved with an outstanding capacity retention ratio of 73.6%, corresponding to a small capacity decay of 0.026% per cycle, proving its highly stable Li-ion insertion and extraction (Figure 3e). To understand the outstanding performance of B-PTCDA cathodes, cyclic voltammetry (CV) has been carried out to investigate the electrochemical reaction kinetics (Figures 3f and S5). The CV curves show two pairs of reversible redox peaks at 2.35/2.69 V and 2.16/2.81 V, indicating a two-electron reaction step of B-PTCDA with Li ions. The relationship between the peak currents and scan rates indicates that the kinetics of B-PTCDA is primarily surface-controlled intercalation pseudocapacitive (Figure 3g). At the high scan rate of 20 mV s^{-1}, the calculated ratio of pseudocapacitive contribution to the total capacity is about 98.3%, which is beneficial for its excellent rate performance (Figure 3h).

In view of the excellent electrochemical performance at room temperature, we further verified the superiority of B-PTCDA for the low temperature operation. At −40 °C, the B-PTCDA cathode delivers a high reversible capacity of 71.8 mAh g^{-1} at 0.2 C, corresponding to a capacity retention of 55% at room temperature (Figure 4a). Moreover, an excellent rate capability (10 C) of B-PTCDA cathode is still maintained at low temperature. The power retention at −40 °C with various rates is presented in comparison with that at room temperature (25 °C). The high power retentions of 91.3%, 82.9% and 75.0% are achieved at 0.1 C, 5 C and 10 C, respectively, demonstrating the superior rate ability of B-PTCDA at low temperature (Figure 4b). Furthermore, an outstanding cycle stability of B-PTCDA cathode is achieved at −40 °C as well. After 100 cycles, the battery exhibits a high capacity retention of 99.5%, presenting a negligible capacity fading (Figure 4c). Such an outstanding cyclic stability is mainly attributed to the intrinsic flexibility of organic B-PTCDA and the stability derived from π-conjugated system. To probe the kinetics change of the B-PTCDA cathode as the temperature drops from 25 °C to −40 °C, the temperature-dependent electrochemical impedance spectroscopy (EIS) was conducted (Figure 4d). The resistance increases as the temperature decreases and the charge transfer resistance becomes much larger than that at room temperature. Moreover, the activation energy (E_a) is calculated from the relationship of $1/R_{ct} = A_0 e^{-Ea/RT}$ (where A_0, R and T correspond to the frequency factor, the gas constant and the Kelvin temperature, respectively), which represents the barrier for the

Research Article
doi.org/10.1002/batt.202200458
Chemistry Europe
European Chemical Societies Publishing

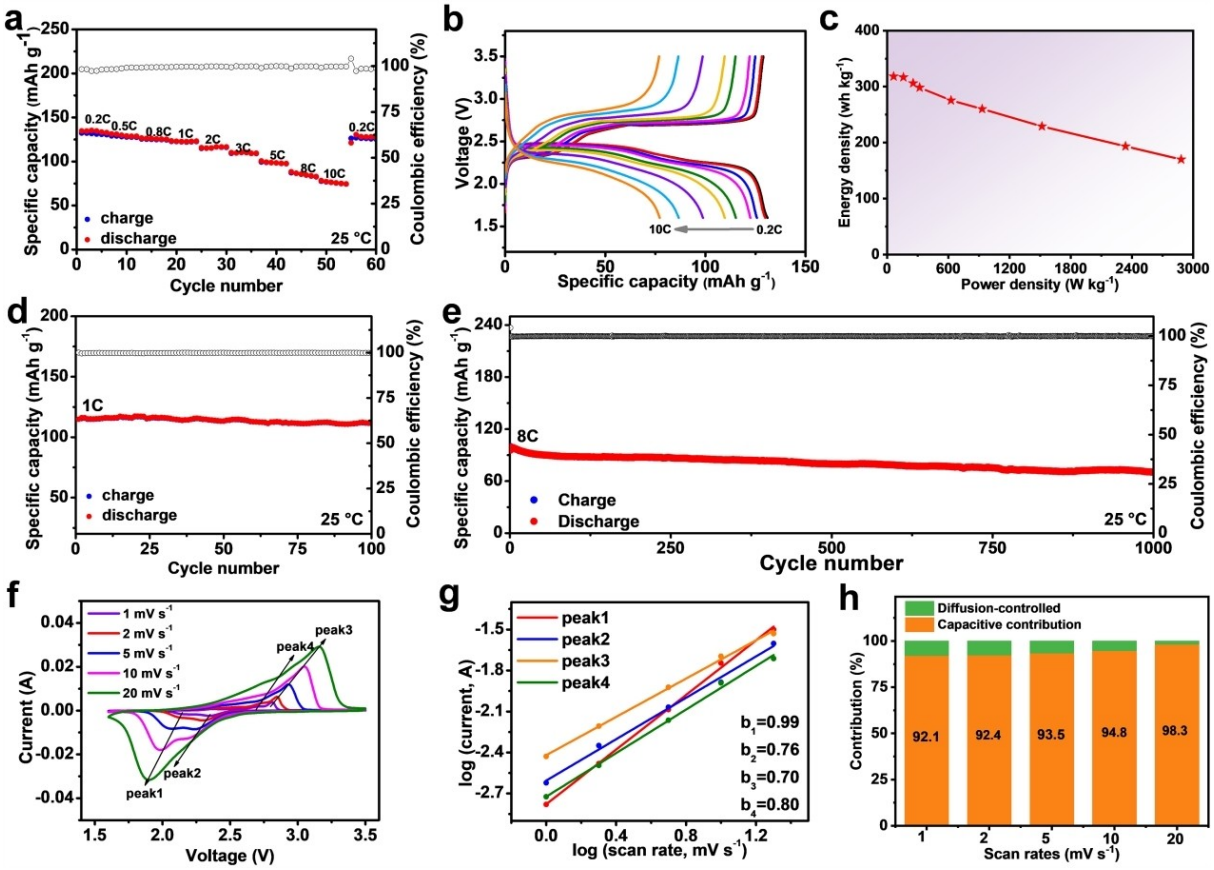

Figure 3. a) Rate performance of B-PTCDA at 25 °C. b) Corresponding GCD curves at 25 °C. c) Ragone plot of B-PTCDA at 25 °C. Cycle performance of B-PTCDA at the rates of d) 1 C and e) 8 C at 25 °C. f) CV curves of B-PTCDA at different scan rates from 1 to 20 mV s^{-1}. g) Relationship between peak currents and scan rates of the CV curves. h) Ratio of pseudocapacitive contribution at different scan rates.

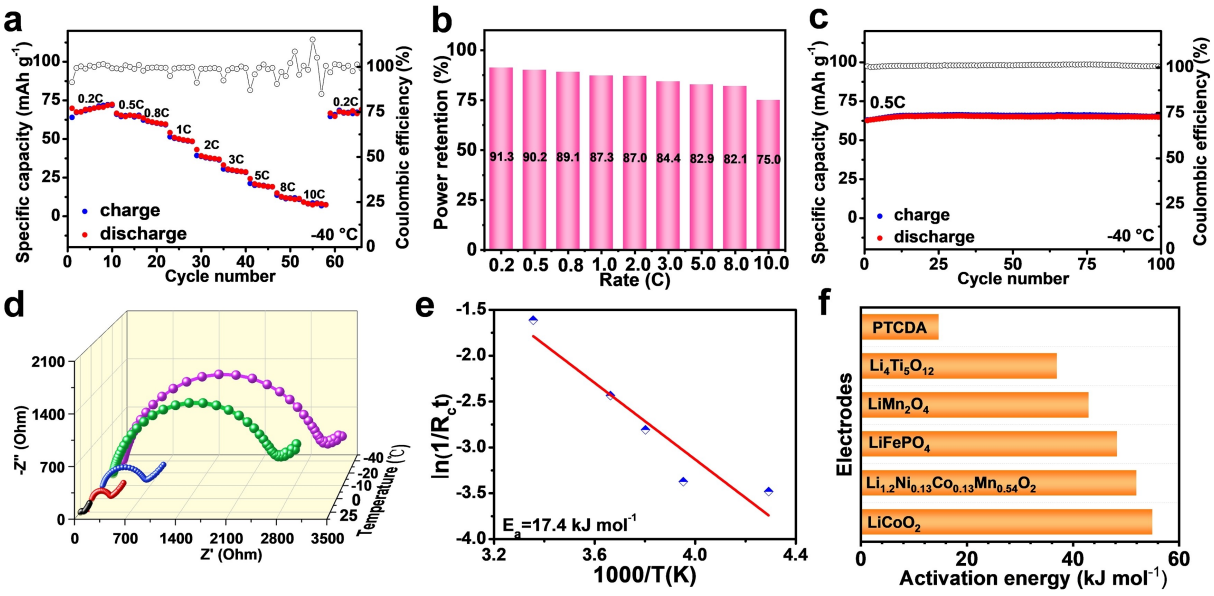

Figure 4. a) Rate performance of B-PTCDA at −40 °C. b) Retention of the power density at −40 °C compared to that obtained at 25 °C. c) Cycle performance of B-PTCDA at 40 °C. d) Nyquist plots of Li||B-PTCDA battery at different temperatures. e) The plot of ln($1/R_{ct}$) and 1000/T to calculate E_a value for B-PTCDA. f) E_a values of B-PTCDA and various commercial electrode materials.

Research Article
doi.org/10.1002/batt.202200458
Chemistry Europe
European Chemical Societies Publishing

Li ion charge transfer processes (Figure 4e).[32] The E_a for B-PTCDA is calculated as 14.7 kJ mol^{-1} by the relation between ln(1/R_{ct}) and (1000/T) (Figure 4f), which is much lower than that of many commercial cathode materials, such as $LiFePO_4$, $LiCoO_2$ and $LiMn_2O_4$.[36–39] Such a small E_a value, combined with the π-conjugated system, enables the excellent low temperature performance of B-PTCDA, which offers a possibility of high mass loading for high-areal-capacity of LIBs.

As a proof of concept, with a high mass loading of 14.35 mg cm^{-2}, the B-PTCDA cathode reaches an areal capacity as high as 1.52 mAh cm^{-2} (0.2 C), as well as a stable cycling performance at 25 °C (Figure 5a). As the temperature is decreased down to −40 °C, a high areal capacity of 1.06 mAh cm^{-2} is still delivered with obvious voltage platforms, indicating a good charge/discharge ability at low temperature (Figures 5b, c and S7). Moreover, at −40 °C, the battery with such high B-PTCDA loading also exhibits a good cyclic stability over 50 cycles at 0.2 C with a high capacity retention of around 90% (Figures 5d and S8). Such a high areal capacity at −40 °C outperforms many previous works about LIBs at low temperatures (Figure 5e).[40–53]

Conclusion

In conclusion, we present a high-areal-capacity LIBs with outstanding low temperature performances by employing organic B-PTCDA as the cathode. This is attributed to the synergistic effect of 1) the charge storage process on the surface groups of B-PTCDA facilitates the rapid Li-ions storage, 2) the delocalization of electrons in the π-conjugated systems of B-PTCDA leads to a high electronic conductivity within the conjugated area. Moreover, the activation energy of B-PTCDA for charge transfer is as low as 14.7 kJ mol^{-1}, which facilitates the fast kinetics of charge transfer even at low temperature. As a result, at a high mass loading of 14.35 mg cm^{-2}, a high areal capacity of 1.06 mAh cm^{-2} is achieved at −40 °C, outperforming many reported low temperature LIBs. This work demonstrates that the π-conjugated organics as electrode materials are

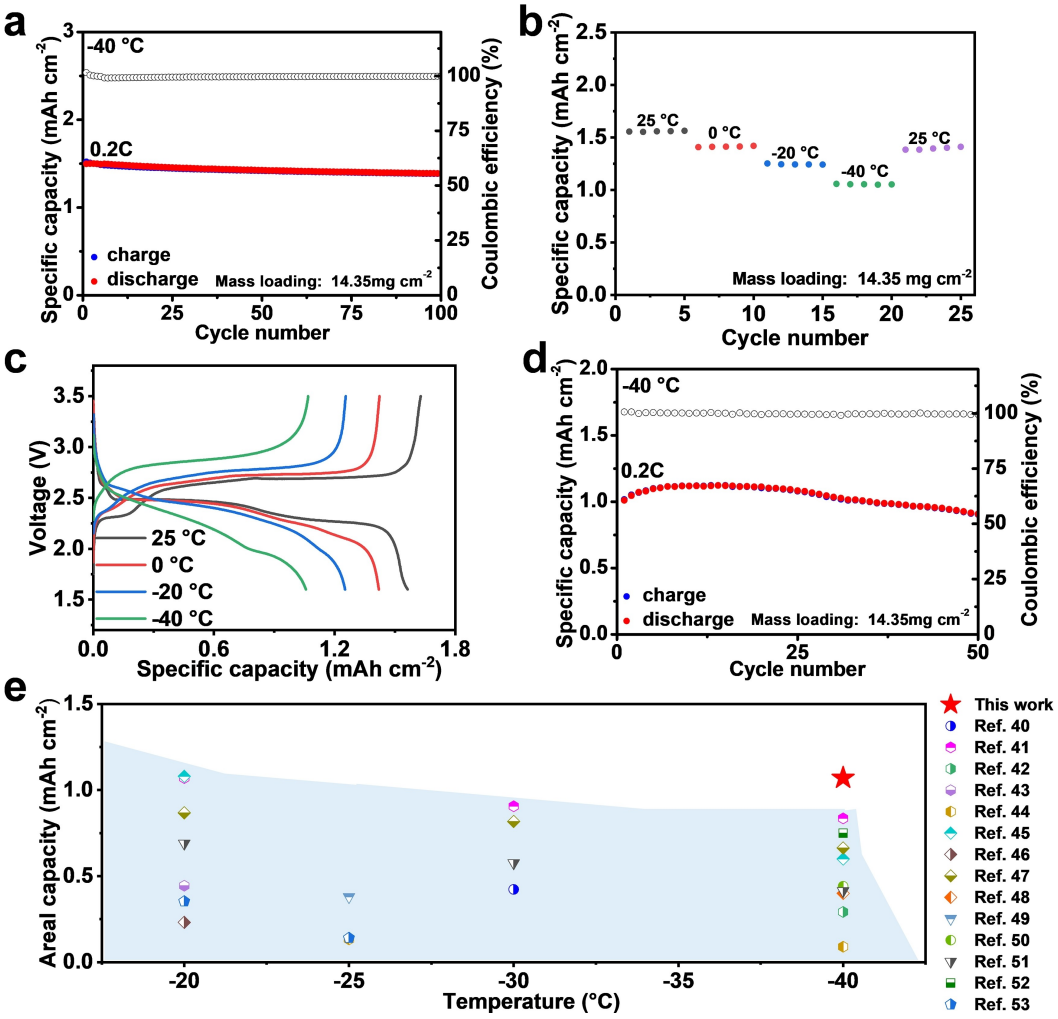

Figure 5. a) Cycle performance of B-PTCDA at 25 °C with a high areal mass loading of 14.35 mg cm^{-2}. b) Galvanostatic cycling of B-PTCDA cathode at different temperatures with an ultrahigh areal mass loading of 14.35 mg cm^{-2}. c) Corresponding GCD curves. d) Cycle performance of B-PTCDA at −40 °C with a high areal mass loading of 14.35 mg cm^{-2}. e) Areal capacity of B-PTCDA cathode at low temperatures in comparison with the reported batteries.

effective for low temperature and high-areal-capacity rechargeable LIBs.

Experimental Section

Preparation of electrolytes and electrodes

For the electrolyte preparation, methyl propionate (MP) was purchased from Sigma-Aldrich. Fluoroethylene carbonate (FEC) and bis(fluorosulfonyl)imide (LiFSI) were purchased from Aladdin. Lithium foils were purchased from DodoChem. Solvents used for electrolyte were dried by adding molecular sieve for at least 24 h. The electrolyte was prepared in an argon-filled glove box ($O_2 <$ 0.01 ppm, $H_2O <$ 0.01 ppm, Mikrouna) by dissolving 1 M LiFSI in MP/FEC (9 : 1 by volume).

For electrodes preparation, perylene-3,4,9,10-tetracarboxylic dianhydride (R-PTCDA) was purchased from Sigma-Aldrich. The B-PTCDA was prepared by annealing R-PTCDA at 450 °C for 5 h under Ar atmosphere with a heating rate of 5 °C min^{-1}.The electrodes were fabricated by mixing R-PTCDA or B-PTCDA, Super P and carboxyl methyl cellulose (CMC, Shenzheng Kejing) with a mass ratio of 7 : 2 : 1 in deionized water followed by casting on Al current collector. The typical average loading mass of the active materials on each cell is around 2 mg cm^{-2} and high mass loading of 14.35 mg cm^{-2} was also prepared.

Electrochemical measurements

CR2032-type cells were used for electrochemical measurements and all the batteries were assembled in an argon-filled glove box. The separators are Celgard 2325 films and the electrolyte for each cell is around 50 μL. GCD measurements were carried out on a CT3001A Land battery testing system (LAND Electronic). Electrochemical impedance spectroscopy (EIS) measurements were performed on a Solartron 1470E electrochemical workstation (AMETEK). All the measurements of the batteries at different temperatures were carried out in a high/low temperature test chamber (Dongguan Qinzhuo Environmental Testing Equipment Co.). All the batteries were placed into a chamber at different temperatures for 2 h before operation.

Characterization

The XRD data were acquired using a Bruker D8 Discover with a step size of 5° min^{-1}. Fourier transform infrared spectroscopy (FTIR) of PTCDA was collected in a Bruker Lumos II with an attenuated total reflection (ATR) module. The X-ray photoelectron spectra (XPS) characterizations were carried out on a Thermo Scientific ESCALAB 250Xi. The morphologies of PTCDA were recorded by a field emission scanning electron microscope (JMS-7500F).

Computational details

The Density functional theory (DFT) calculations for PTCDA were performed in a Gaussian 09 D.01 program package using the Lee-Yang-Parr correlation functional (B3LYP) combined with 6-311G* basis set. Based on the optimized structure of PTCDA molecules, ESP analysis on the van der Waals surface with the Multiwfn 3.6 software package. The current density susceptibility for PTCDA was calculated by Gaussian 09 and the gauge including magnetically induced current method (GIMIC model, as implemented in the GIMIC 2.1.4 code.[54–56]

Supporting Information

Supporting Information is available from the Wiley Online Library or from the author.

Acknowledgements

The authors acknowledge the financial support of the National Natural Science Foundation of China (21972007, 52172178 and 51902013), the Natural Science Foundation of Beijing (2222059) and Jian-Hua Research Foundation of Hebei University of Technology (HB1921 and HB1920). This research was supported by the high-performance computing (HPC) resources at Beihang University.

Conflict of Interest

The authors declare no conflict of interest.

Data Availability Statement

The data that support the findings of this study are available from the corresponding author upon reasonable request.

Keywords: areal capacity · high mass loading · lithium battery · low temperature · organic electrode

[1] C. Zhang, F. Wang, J. Han, S. Bai, J. Tan, J. Liu, F. Li, *Small Structures* **2021**, *2*, 2100009.
[2] S. Dong, D. Yu, J. Yang, L. Jiang, J. Wang, L. Cheng, Y. Zhou, H. Yue, H. Wang, L. Guo, *Adv. Mater.* **2020**, *32*, 1908027.
[3] A. Molina, N. Patil, E. Ventosa, M. Liras, J. Palma, R. Marcilla, *ACS Energy Lett.* **2020**, *5*, 2945.
[4] L. Fan, R. Ma, J. Wang, H. Yang, B. Lu, *Adv. Mater.* **2018**, *30*, 1805486.
[5] J. Chen, D. Yu, Q. Zhu, X. Liu, J. Wang, W. Chen, R. Ji, K. Qiu, L. Guo, H. Wang, *Adv. Mater.* **2022**, *34*, 2205678.
[6] W. Zhang, Y. Lu, L. Wan, P. Zhou, Y. Xia, S. Yan, X. Chen, H. Zhou, H. Dong, K. Liu, *Nat. Commun.* **2022**, *13*, 2029.
[7] B. Nan, L. Chen, N. D. Rodrigo, O. Borodin, N. Piao, J. Xia, T. Pollard, S. Hou, J. Zhang, X. Ji, J. Xu, X. Zhang, L. Ma, X. He, S. Liu, H. Wan, E. Hu, W. Zhang, K. Xu, X. Q. Yang, B. Lucht, C. Wang, *Angew. Chem. Int. Ed.* **2022**, *61*, 2205967.
[8] X. Shangguan, G. Xu, Z. Cui, Q. Wang, X. Du, K. Chen, S. Huang, G. Jia, F. Li, X. Wang, D. Lu, S. Dong, G. Cui, *Small* **2019**, *15*, 1900269.
[9] J. Zhou, Y. Wang, J. Wang, Y. Liu, Y. Li, L. Cheng, Y. Ding, S. Dong, Q. Zhu, M. Tang, Y. Wang, Y. Bi, R. Sun, Z. Wang, H. Wang, *Energy Storage Mater.* **2022**, *50*, 47.
[10] M. Shang, X. Chen, B. Li, J. Niu, *ACS Nano* **2020**, *14*, 3678.
[11] T. Ma, Y. Ni, Q. Wang, W. Zhang, S. Jin, S. Zheng, X. Yang, Y. Hou, Z. Tao, J. Chen, *Angew. Chem. Int. Ed.* **2022**, *61*, 2207927.
[12] R. Zhao, N. Sun, B. Xu, *Small Structures* **2021**, *2*, 2100132.
[13] N. Zhang, T. Deng, S. Zhang, C. Wang, L. Chen, C. Wang, X. Fan, *Adv. Mater.* **2022**, *34*, 2107899.
[14] K. Du, E. H. Ang, X. Wu, Y. Liu, *Energy Environ. Mater.* **2022**. DOI: 10.1002/eem2.12271.
[15] D. Yu, Q. Zhu, L. Cheng, S. Dong, X. Zhang, H. Wang, N. Yang, *ACS Energy Lett.* **2021**, *6*, 949.
[16] V. V. T. Doan-Nguyen, S. Zhang, E. B. Trigg, R. Agarwal, J. Li, D. Su, K. I. Winey, C. B. Murray, *ACS Nano* **2015**, *9*, 8108.
[17] S.-T. Guo, S.-X. Zhao, K. Bi, Y.-F. Deng, K. Xiong, C.-W. Nan, *Electrochim. Acta* **2016**, *222*, 1733.

[18] X. Dong, Z. Guo, Z. Guo, Y. Wang, Y. Xia, *Joule* **2018**, *2*, 902.
[19] X. Feng, X. Chen, B. Ren, X. Wu, X. Huang, R. Ding, X. Sun, S. Tan, E. Liu, P. Gao, *ACS Appl. Mater. Interfaces* **2021**, *13*, 7178.
[20] M. Li, J. Yang, Y. Shi, Z. Chen, P. Bai, H. Su, P. Xiong, M. Cheng, J. Zhao, Y. Xu, *Adv. Mater.* **2022**, *34*, 2107226.
[21] J. Qin, Q. Lan, N. Liu, Y. Zhao, Z. Song, H. Zhan, *Energy Storage Mater.* **2020**, *26*, 585.
[22] T. Sun, Q.-Q. Sun, Y. Yu, X.-B. Zhang, *eScience* **2021**, *1*, 186.
[23] Z. He, J. Zhang, X. Guo, H. Kang, Z. Wang, Y. Liu, M. Wang, H. Zhang, *Small Structures* **2021**, *2*, 2100108.
[24] Y. Liang, Z. Tao, J. Chen, *Adv. Energy Mater.* **2012**, *2*, 742.
[25] Y. Zhang, L. Zhao, Y. Liang, X. Wang, Y. Yao, *eScience* **2022**, *2*, 110.
[26] M. Tang, Q. Zhu, P. Hu, L. Jiang, R. Liu, J. Wang, L. Cheng, X. Zhang, W. Chen, H. Wang, *Adv. Funct. Mater.* **2021**, *31*, 2102011.
[27] L. Cheng, Q. Zhu, J. Liang, M. Tang, Y. Yang, S. Wang, P. Ji, G. Wang, W. Chen, X. Zhang, H. Wang, *ACS Appl. Mater. Interfaces* **2021**, *13*, 54096.
[28] Z. Tie, S. Deng, H. Cao, M. Yao, Z. Niu, J. Chen, *Angew. Chem. Int. Ed.* **2022**, *61*, 2115180.
[29] Y. Lu, Y. Cai, Q. Zhang, J. Chen, *Adv. Mater.* **2022**, *34*, 2104150.
[30] P. Cai, G. Wang, K. Chen, Z. Wen, *J. Power Sources* **2019**, *428*, 37.
[31] X. Han, C. Chang, L. Yuan, T. Sun, J. Sun, *Adv. Mater.* **2007**, *19*, 1616.
[32] W. Luo, M. Allen, V. Raju, X. Ji, *Adv. Energy Mater.* **2014**, *4*, 1400554.
[33] G. Zhou, Y.-E. Miao, Z. Wei, L. Mo, F. Lai, Y. Wu, J. Ma, T. Liu, *Adv. Funct. Mater.* **2018**, *28*, 1804629.
[34] M. Hara, A. Satoh, N. Takami, T. Ohsaki, *J. Phys. Chem.* **1995**, *99*, 16338.
[35] Y. Huang, R. Yuan, S. Zhou, *J. Mater. Chem.* **2012**, *22*, 883.
[36] X. Dong, Y. Yang, P. Li, Z. Fang, Y. Wang, Y. Xia, *Batteries & Supercaps* **2020**, *3*, 1016.
[37] A. Yano, K. Hikima, J. Hata, K. Suzuki, M. Hirayama, R. Kanno, *J. Electrochem. Soc.* **2018**, *165*, A3221.
[38] A. A. Kuz'mina, T. L. Kulova, E. K. Tuseeva, E. V. Chirkova, *Russ. J. Electrochem.* **2020**, *56*, 899.
[39] G. Wang, H. Kang, M. Chen, K. Yan, X. Hu, E. J. Cairns, *ChemElectroChem* **2017**, *4*, 376.
[40] Y. Yang, Z. Fang, Y. Yin, Y. Cao, Y. Wang, X. Dong, Y. Xia, *Angew. Chem. Int. Ed.* **2022**, *61*, 2208345.
[41] S. Tan, L. Wang, L. Bian, J. Xu, W. Ren, P. Hu, A. Chang, *J. Power Sources* **2015**, *277*, 139.
[42] Y. Wang, H. Zheng, L. Hong, F. Jiang, Y. Liu, X. Feng, R. Zhou, Y. Sun, H. Xiang, *Chem. Eng. J.* **2022**, *445*, 136802.
[43] Z. Sun, Z. Li, L. Gao, X. Zhao, D. Han, S. Gan, S. Guo, L. Niu, *Adv. Energy Mater.* **2018**, *9*, 1802946.
[44] X. Cui, K. Tuo, Y. Xie, C. Li, D. Zhao, L. Yang, X. Fu, S. Li, *Ionics* **2020**, *26*, 3795.
[45] X. Shangguan, G. Xu, Z. Cui, Q. Wang, X. Du, K. Chen, S. Huang, G. Jia, F. Li, X. Wang, D. Lu, S. Dong, G. Cui, *Small* **2019**, *15*, 1900269.
[46] K. S. Chen, R. Xu, N. S. Luu, E. B. Secor, K. Hamamoto, Q. Li, S. Kim, V. K. Sangwan, I. Balla, L. M. Guiney, J. T. Seo, X. Yu, W. Liu, J. Wu, C. Wolverton, V. P. Dravid, S. A. Barnett, J. Lu, K. Amine, M. C. Hersam, *Nano Lett.* **2017**, *17*, 2539.
[47] W. Lv, C. Zhu, J. Chen, C. Ou, Q. Zhang, S. Zhong, *Chem. Eng. J.* **2021**, *418*,129400.
[48] Y. Yang, P. Li, N. Wang, Z. Fang, C. Wang, X. Dong, Y. Xia, *Chem. Commun.* **2020**, *56*, 9640.
[49] T. Feng, G. Yang, S. Zhang, Z. Xu, H. Zhou, M. Wu, *Chem. Eng. J.* **2022**, *433*, 134138.
[50] S. Kim, B. Seo, H. V. Ramasamy, Z. Shang, H. Wang, B. M. Savoie, V. G. Pol, *ACS Appl. Mater. Interfaces* **2022**, *14*, 41934.
[51] A. Pan, Z. Wang, F. Zhang, L. Wang, J. Xu, J. Zheng, J. Hu, C. Zhao, X. Wu, *Nano Res.* **2022**, doi:org/10.1007/s12274-022-4655-1.
[52] S. Lin, H. Hua, P. Lai, J. Zhao, *Adv. Energy Mater.* **2021**, *11*, 2101775.
[53] Z. Piao, P. Xiao, R. Luo, J. Ma, R. Gao, C. Li, J. Tan, K. Yu, G. Zhou, H. M. Cheng, *Adv. Mater.* **2022**, *34*, 2108400.
[54] M. J. Frisch, G. W. Trucks, H. B. Schlegel, G. E. Scuseria, M. A. Robb, J. R. Cheeseman, G. Scalmani, V. Barone, B. Mennucci, G. A. Petersson, H. Nakatsuji, M. Caricato, X. Li, H. P. Hratchian, A. F. Izmaylov, J. Bloino, G. Zheng, J. L. Sonnenberg, M. Hada, M. Ehara, K. Toyota, R. Fukuda, J. Hasegawa, M. Ishida, T. Nakajima, Y. Honda, O. Kitao, H. Nakai, T. Vreven, J. A. Montgomery, Jr., J. E. Peralta, F. Ogliaro, M. Bearpark, J. J. Heyd, E. Brothers, K. N. Kudin, V. N. Staroverov, T. Keith, R. Kobayashi, J. Normand, K. Raghavachari, A. Rendell, J. C. Burant, S. S. Iyengar, J. Tomasi, M. Cossi, N. Rega, J. M. Millam, M. Klene, J. E. Knox, J. B. Cross, V. Bakken, C. Adamo, J. Jaramillo, R. Gomperts, R. E. Stratmann, O. Yazyev, A. J. Austin, R. Cammi, C. Pomelli, J. W. Ochterski, R. L. Martin, K. Morokuma, V. G. Zakrzewski, G. A. Voth, P. Salvador, J. J. Dannenberg, S. Dapprich, A. D. Daniels, O. Farkas, J. B. Foresman, J. V. Ortiz, J. Cioslowski, D. J. Fox, Gaussian 09, Revision D.01, Gaussian, Inc., Wallingford CT, 2013.
[55] G. Kresse, J. Furthmüller, *J. Comput. Mater. Sci.* **1996**, *6*, 15.
[56] K. Momma, F. Izumi, *J. Appl. Crystallogr.* **2011**, *44*, 1272.

Manuscript received: October 19, 2022
Revised manuscript received: November 21, 2022
Accepted manuscript online: November 29, 2022
Version of record online: December 7, 2022